The Temperature-Humidity Covariance Budget in the Convective Boundary Layer

J. C. WYNGAARD

Cooperative Institute for Research in Environmental Sciences, University of Colorado/NOAA, Boulder 80309, and Wave Propagation Laboratory, NOAA, Boulder, Colo. 80302

W. T. PENNELL,[2] D. H. LENSCHOW AND M. A. LEMONE

National Center for Atmospheric Research,[1] Boulder, Colo. 80307

(Manuscript received 27 May 1977, in final form 30 September 1977)

The behavior of the temperature-humidity covariance ($\overline{\theta q}$) budget in the convectively driven boundary layer is determined through analysis of data from AMTEX and (to a lesser extent) Kansas and Minnesota. In the near-neutral surface layer a balance is found between production and molecular destruction; in the mixed layer, transport is also important. We extend the Corrsin theory for inertial subrange scalar spectral behavior to the temperature-humidity cospectrum, and thus relate the molecular destruction rate of $\overline{\theta q}$ to its inertial range level. Destruction rates inferred from AMTEX cospectra agree with those found from the imbalance of production and transport terms. The budgets within the surface layer and the mixed layer are parameterized separately with appropriate scales.

Both temperature and humidity fluctuations contribute to the small-scale refractive index variations which affect acoustic and electromagnetic wave propagation in the atmosphere. Our results indicate that their joint contribution C_{Tq} to the refractive index structure parameter is directly related to the molecular destruction rate of $\overline{\theta q}$. The results provide a basis for understanding and predicting the behavior of C_{Tq} in the convective boundary layer.

1. Introduction

A convective boundary layer over an evaporating surface has significant fluctuation levels in both temperature and humidity. It has long been observed that these fluctuations can be strongly correlated. The mechanisms through which a turbulent flow maintains strong scalar-scalar correlations are of interest in their own right, and have relevance to a range of disciplines from turbulent chemistry to wave propagation through turbulence.

In the latter application, for example, Gossard (1960) and more recently Friehe *et al.* (1975) and Wesely (1976) have shown how both temperature and humidity fluctuations contribute to refractive index fluctuations. One can write

$$n=-C(\theta+aq), \tag{1}$$

where n, θ and q are fluctuating refractive index, temperature and absolute humidity (units of grams of water vapor per cubic meter), respectively, and C is a conversion constant which we will ignore hereafter. The factor a depends on the wavelength of the acoustic or electromagnetic radiation. In calculating turbulence effects on wave propagation one usually deals with the refractive index structure function (Tatarskii, 1971)

$$\overline{[n(\mathbf{x},t)-n(\mathbf{x}+\mathbf{r},t)]^2}\equiv\overline{(n-n')^2}, \tag{2}$$

where n is measured at $\mathbf{x}$ and n' at $\mathbf{x}+\mathbf{r}$. From Eq. (1) this is

$$\overline{(n-n')^2}=\overline{(\theta-\theta')^2}+2a\overline{(\theta-\theta')(q-q')}+a^2\overline{(q-q')^2}. \tag{3}$$

For separation magnitudes r in the inertial range ($\eta\ll r\ll l$, where η is the Kolmogorov microscale and l the integral scale), locally isotropic, Kolmogorov-Corrsin turbulence is usually assumed. Then structure functions depend on r, not $\mathbf{r}$, so that Eq. (3) can be written

$$\overline{(n-n')^2}=2\overline{\theta^2}\left(1-\frac{\overline{\theta\theta'}}{\overline{\theta^2}}\right)+4a\overline{\theta q}\left(1-\frac{(\overline{\theta q'}+\overline{\theta' q})}{2\overline{\theta q}}\right)+2a^2\overline{q^2}\left(1-\frac{\overline{qq'}}{\overline{q^2}}\right) \tag{4}$$

[1] The National Center for Atmospheric Research is sponsored by the National Science Foundation.

[2] Present affiliation: Battelle Pacific Northwest Laboratories, Richland, Wash. 99352.

0022-4928/78/0047-0058$06.00

TABLE 1. Values of surface layer scaling parameters, surface virtual temperature flux and mixed layer depth for AMTEX 1975 flights.

Date	z_i (m)	u_* (m s^{-1})	$-T_*$ (K)	$-q_*$ (g m^{-3})	Q_{0v} (m s^{-1} K)	$-L$ (m)
2/15	1200	0.53	0.26	0.28	0.16	76
2/16	1430	0.40	0.28	0.35	0.13	40
2/18	1010	0.35	0.17	0.40	0.08	44
2/22	1900	0.58	0.34	0.52	0.24	67
2/24	1200	0.30	0.25	0.67	0.10	22
2/26	680	0.33	0.12	0.29	0.05	59

and the temperature and humidity structure functions behave as

$$\overline{(\theta-\theta')^2}=2\bar{\theta}^2\left(1-\frac{\overline{\theta\theta'}}{\bar{\theta}^2}\right)=C_T^2r^{\frac{2}{3}}, \tag{5}$$

$$\overline{(q-q')^2}=2\bar{q}^2\left(1-\frac{\overline{qq'}}{\bar{q}^2}\right)=C_q^2r^{\frac{2}{3}}, \tag{6}$$

where C_T^2 and C_q^2 are the temperature and humidity structure parameters. We will show here that the cross term in Eq. (4) also has this r-dependence, so that one can write

$$C_n^2=C_T^2+2aC_{Tq}+a^2C_q^2 \tag{7}$$

as has often been implicity assumed in past literature. We will also show that C_{Tq} is directly related to the molecular destruction term in the $\overline{\theta q}$ budget. Our budget results thus provide a basis for relating C_{Tq} to other turbulence quantities in the convective boundary layer.

2. Measurements

The airplane measurements reported here were made with the NCAR Lockheed Electra over the East China Sea as part of the Air Mass Transformation Experiment (AMTEX) during February 1975. Table 1 is a summary of the surface fluxes and certain boundary layer parameters for the six AMTEX boundary layer flights. Except for those on 24 and 26 February, the measurements were obtained during periods of cold air advection over the Kuroshio, a warm, northward flowing ocean current. Under conditions of strong cold air advection the convectively unstable boundary layer is capped by a well-defined inversion layer at height z_i, usually 1–2 km above the surface, with broken decks of stratocumulus clouds in the upper few hundred meters. On 24 February the mixed layer was also capped by stratocumulus but the inversion was quite weak and surface winds were southwesterly. Conditions on 26 February were like those commonly observed over tropical oceans. Winds were light, the air-sea temperature contrast was small, and the mixed-layer height was about cloud base for the scattered to broken cumulus observed in the area of measurements.

Fig. 1 shows profiles of mean potential temperature and humidity that were typical for the conditions of strong cold air advection. These profiles are made up of both aircraft soundings (i.e., constant heading descents or ascents at about 5 m s^{-1}) and "leg average" values over 60 km long straight and level flight paths. Profiles on 24 and 26 February were similar except that the jumps in Θ and Q were much less pronounced and z_i was more difficult to determine.

The Electra air motion sensing system uses an inertial navigation system (INS) to measure the velocity and angular orientation of the airplane relative to the earth. The longitudinal component of air velocity with respect to the airplane (the aircraft true airspeed) is measured by means of a pitot-static tube, while the lateral and vertical components are measured by means of vanes. These sensors are mounted on a nose boom about 6 m ahead of the aircraft to reduce the error caused by upwash effects on air flow around the fuselage. The air velocity measurements with respect to the airplane are combined with the INS outputs to obtain the three air velocity components relative to the earth, as described by Lenschow (1972).

Temperature is measured with a 25 μm platinum resistance wire thermometer (Rosemount Model No. 102E2AL). The sensor output is corrected for dynamic heating, which is proportional to the square of the aircraft true airspeed. Since the aircraft altitude varies somewhat due to turbulence and pilot control inputs, the temperature measured from the aircraft can be affected by the mean lapse rate. As shown in Fig. 1, the mean potential temperature lapse rate is close to zero. Therefore, potential temperature fluctuations (calculated from temperature and static pressure) are actually used instead of temperature in all the measurements discussed here. In order to convert potential temperature fluctuations to temperature fluctuations, they must be multiplied by the ratio of mean temperature to mean potential temperature. This was not done here since this factor never departed from unity by more than 7%.

Absolute humidity is measured with a cooled-mirror dew-point hygrometer. Both a fixed-path Lyman-alpha hygrometer (LAH) [Buck (1976) describes a variable-path version of this sensor] and a microwave refractometer (McGavin and Vetter, 1965) are used for humidity fluctuation measurements. The LAH was used for all of the humidity fluctuation measurements except for the lowest flight level on 15 February 1975, when the LAH was off-scale, because the refractometer was noisier at high frequencies. The effect of this electronic noise on the data reported here is negligible.

With the exception of the LAH, all of the sensors measuring turbulent fluctuations in the airstream are

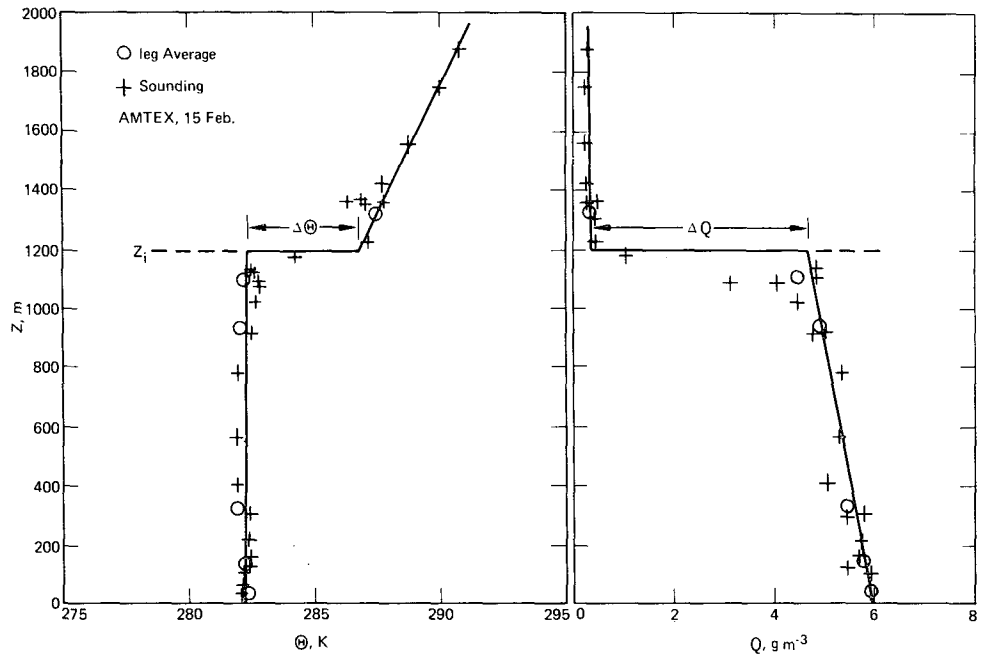

FIG. 1. Typical profiles of mean potential temperature Θ and mean absolute humidity Q during AMTEX. Note the well-defined inversion base at z_i and the jumps $\Delta\Theta$ and ΔQ there.

within a meter of each other on the aircraft nose boom. The LAH is located on the nose boom about 3 m downstream from the other sensors. To compensate for this (which amounts to about 0.03 s delay time) and for the lag introduced by the reduced velocity of the air in the 0.37 m length of tubing upstream from the sensor, the sensor output is advanced by one time interval (0.05 s) with respect to the other variables. The remaining 0.02 s delay is equivalent to a velocity in the hygrometer tubing of 18 m s^{-1}. This seems reasonable in view of the bends in the tubing and the obstruction at the entrance to the tube, which is intended to help keep the sensor free from water by deflecting hydrometeors away from the entrance. The magnitude of this phase advancement was determined by minimizing the phase angle at high frequencies between humidity and vertical velocity w. Vertical velocity, which is used as a reference for phase shift comparisons, is measured with sensors that have negligible phase shift over the bandwidth used for these calculations. Similarly, the LAH response, disregarding the effects of location and ducting, is assumed to have negligible phase shift and attenuation over the bandwidth considered here. The phase angle relationships between humidity, temperature and vertical velocity were found to be independent of the heading of the aircraft with respect to the wind direction to verify that these are instrumental characteristics rather than real physical relationships existing in the atmosphere.

The temperature response, however, has significant phase shift and attenuation. Because of heat conduction between the wire and its housing, the temperature response is not describable by a simple, linear, first-order differential equation with a single time constant characteristic of the resistance wire. McCarthy (1973) attempted to model its response by assuming that its response to ambient air temperature fluctuations can be approximated by the smoothing or filtering function

$$0.7e^{-t/\tau_1}+0.3e^{-t/\tau_2}. \tag{8}$$

The first term represents the response of the sensing element, and the second term is due to heat conduction between the element and its supporting structure which has much greater thermal inertia. McCarthy used the values $\tau_1=0.016$ s and $\tau_2=1.15$ s, which he obtained from the manufacturer. However, measurements from the Electra indicate that a value of $\tau_1=0.03$ s gives better agreement with the observed phase shifts of θ and w, as well as θ and q.

With the exception of the two INS horizontal airplane velocity components, which were recorded at 10 samples per second, the Electra turbulence data were recorded at 50 samples per second. All the variables were low-pass filtered with either analog or digital 4-pole low-pass Butterworth filters with a cutoff frequency of about 10 Hz and then interpolated to a sampling rate of 20 samples per second.

The overland humidity statistics reported here were measured during the 1973 Minnesota experiments, using equipment and techniques described in detail by Champagne *et al.* (1977).

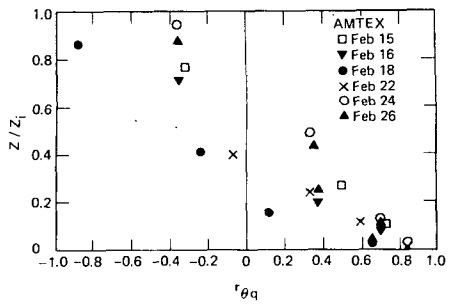

FIG. 2. Vertical profiles of $r_{\theta q}$, the correlation coefficient of temperature and humidity fluctuations, during AMTEX.

3. The $\overline{\theta q}$ budget

It is well-established that $\overline{\theta q}$ is positive above a warm, evaporating surface (Swinbank and Dyer, 1967; Phelps and Pond, 1971; McBean and Miyake, 1972; Friehe *et al.*, 1975; Wesely, 1976). Not as well-documented, but perhaps as physically understandable, are the negative $\overline{\theta q}$ values in the upper portions of the convective ABL. The inversion which typically caps the ABL in these conditions usually has a sharp increase in temperature with height, but a sharp decrease in humidity; thus entrainment leads to large negative $\overline{\theta q}$ values near z_i. Fig. 2, based on data from six days in the AMTEX experiment, shows the vertical profile of the correlation coefficient $r_{\theta q}$, defined by

$$r_{\theta q}=\frac{\overline{\theta q}}{[\overline{\theta^2}\,\overline{q^2}]^{\frac{1}{2}}}. \tag{9}$$

Note from Fig. 2 that $r_{\theta q}$ approaches 1.0 near the surface, changes sign at $z/z_i\approx 0.5$, and can be large and negative near the inversion base.

We can learn much about the maintenance of $\overline{\theta q}$ from its conservation equation, which is derived from those for θ and q. Neglecting radiation and phase change effects (thus restricting our attention to the region below cloud base) the θ equation is (Lumley and Panofsky, 1964)

$$\theta_{,t}+\Theta_{,j}u_j+\theta_{,j}U_j+\theta_{,j}u_j-\overline{\theta_{,j}u_j}=K\theta_{,jj}. \tag{10}$$

Here K is thermal diffusivity, and we denote mean quantities by upper case symbols; a comma denotes differentiation and repeated indices are summed. The q equation is derived by using a mean and turbulent decomposition in the humidity conservation equation. The variable air density introduces many advective terms, but under typical boundary layer conditions most can be neglected. We assume the scale height $h=\rho/(\rho_{,3})\gg l$, where ρ is the mean density and l a characteristic turbulence integral scale. We also assume $(\overline{q^2})^{\frac{1}{2}}/Q\gg(\overline{\theta^2})^{\frac{1}{2}}/T\approx(\overline{\rho'^2})^{\frac{1}{2}}/\rho$, where ρ' is fluctuating density; both are usually excellent approximations. Under these conditions the q equation reduces to

$$q_{,t}+\rho(Q/\rho)_{,j}u_j+q_{,j}U_j+q_{,j}u_j-\overline{q_{,j}u_j}=Dq_{,jj} \tag{11}$$

where D is the diffusivity for q.

Note that the second term in Eq. (10) contains the gradient of mean *potential* temperature, not mean temperature. Thus even though there is a mean vertical gradient of temperature in a neutral ($\Theta_{,3}=0$) atmosphere, vertical velocity fluctuations do not cause temperature fluctuations. Eq. (11) shows an analogous situation exists for humidity. Because ρ decreases with z, a well-mixed layer [$(Q/\rho)_{,3}=0$] will have a mean vertical gradient of absolute humidity, but vertical velocity fluctuations will not generate q fluctuations.

Multiplying the θ equation by q, the q equation by θ, adding and averaging gives in large Reynolds number turbulence (Tennekes and Lumley, 1972)

$$(\overline{\theta q})_{,t}=-\Theta_{,j}\overline{u_jq}-\rho(Q/\rho)_{,j}\overline{u_j\theta}-(U_j\overline{\theta q})_{,j}-(\overline{u_j\theta q})_{,j}-2(K+D)\overline{\theta_{,j}q_{,j}}. \tag{12}$$

The terms on the right side of Eq. (12) are, in order, production through the mean potential temperature gradient, production through the mean specific humidity gradient, mean advection, turbulent transport and molecular destruction.

In the horizontally homogeneous flows we consider here, the $\overline{\theta q}$ budget simplifies to

$$(\overline{\theta q})_{,t}=-\Theta_{,3}\overline{wq}-\rho(Q/\rho)_{,3}\overline{w\theta}-(\overline{w\theta q})_{,3}-2(K+D)\overline{\theta_{,j}q_{,j}}, \tag{13}$$

where we revert to the notation $u_3=w$. We can now discuss the behavior of the horizontally homogeneous budget (13) in two regions of the convective ABL.

4. The unstable surface layer

We consider both $\overline{wq}$ and $\overline{w\theta}$ to be positive, and both $\Theta_{,3}$ and $(Q/\rho)_{,3}$ negative—the normal situation above a warm evaporating surface. Then both the production terms in Eq. (13) create positive $\overline{\theta q}$. We will now argue that in this situation the transport term is much smaller.

Data on $\overline{w\theta q}$ are scarce, but since under the conditions we are considering θ and q are strongly positively correlated, we expect $\overline{w\theta q}$ to behave much like $\overline{w\theta\theta}$. Fig. 3 is a compilation of $\overline{w\theta^2}$ data from Minnesota (Kaimal *et al.*, 1976) and Kansas (Wyngaard and Coté, 1971), and $\overline{w\theta q}$ data from Minnesota (Champagne *et al.*, 1977) and AMTEX. We non-

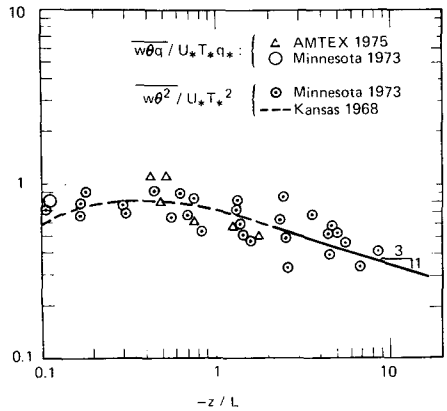

FIG. 3. Data on the vertical fluxes of θ^2 and θq in the surface layer from AMTEX, Minnesota and Kansas.

dimensionalize with the scales

$$\left.\begin{aligned} T_* &= -Q_0/u_* \\ q_* &= -M_0/u_* \\ L &= \frac{-u_*^3 T}{kgQ_{0v}} \end{aligned}\right\}, \tag{14}$$

where Q_0 and M_0 are the surface temperature and moisture fluxes, Q_{0v} is the surface virtual temperature flux $Q_0+(0.61TM_0/\rho)$, and $k=0.35$ (Businger *et al.*, 1971) is the von Kármán constant. The data in Fig. 3, although limited, do support our hypothesis that $\overline{w\theta q}$ and $\overline{w\theta^2}$ behave similarly. Therefore, we will use Fig. 3 to estimate transport of $\overline{\theta q}$ in the unstable surface layer.

Fig. 3 indicates no significant transport in the interval $0.1<-z/L<0.5$. The data for $0.5<-z/L<5$ follow the Kansas local free convection prediction (Wyngaard *et al.*, 1971a)

$$\overline{w\theta^2}=0.75u_*T_*^2(-z/L)^{-\frac{1}{3}}. \tag{15}$$

Assuming this holds for $\overline{w\theta q}$, the transport term in Eq. (13) for $0.5<-z/L<5$ becomes in dimensionless form

$$-(\overline{w\theta q})_{,3}\approx 0.25\frac{u_*T_*q_*}{z}\left(-\frac{z}{L}\right)^{-\frac{1}{3}}. \tag{16}$$

In the surface layer, where $z\ll h$ (where h is the scale height), we have

$$\rho(Q/\rho)_{,3}\approx Q_{,3} \tag{17}$$

and the production terms in Eq. (13) are, in dimensionless form,

$$-\overline{w\theta}\rho(Q/\rho)_{,3}\approx -\overline{w\theta}Q_{,3}=\frac{u_*T_*q_*}{kz}\phi_q \tag{18}$$

$$-\overline{wq}\Theta_{,3}=\frac{u_*T_*q_*}{kz}\phi_h \tag{19}$$

with ϕ_h and ϕ_q the dimensionless mean gradients. We take $\phi_h=\phi_q$ (Businger, 1973) so the two production terms are equal. Businger *et al.* (1971) fit the formula

$$\phi_h=0.74(1-9z/L)^{-\frac{1}{2}} \tag{20}$$

to the Kansas data in the range $0<-z/L<2$, but we will use the expression

$$\phi_h=0.23(-z/L)^{-\frac{1}{3}} \tag{21}$$

which fits the data nearly as well in the range $0.5<-z/L<2$. Then the ratio of transport to production terms for $0.5<-z/L<2$ becomes, from Eqs. (16)–(19) and Eq. (21),

$$\frac{\text{transport}}{\text{production}}\approx 0.2. \tag{22}$$

The ratio is even smaller in the range $0<-z/L<0.5$, assuming the trend in Fig. 3 continues for $-z/L\to 0$.

Thus within an error of about 20% we can neglect transport in the unstable surface layer, giving for $0<-z/L<2$

$$(\overline{\theta q})_{,t}\approx -\Theta_{,3}\overline{wq}-Q_{,3}\overline{w\theta}-2(K+D)\overline{\theta_{,j}q_{,j}}. \tag{23}$$

It is easy to show that $\overline{\theta q}$ would have to change significantly over a time scale $\tau\sim z/u_*$ (about 30 s for $z=10$ m and $u_*=0.3$ m s^{-1}) in order for the time term in Eq. (23) to be important. This does not happen, so we can adopt the quasi-steady budget for $0<-z/L<2$

$$(\overline{\theta q})_{,t}\approx 0\approx -\Theta_{,3}\overline{wq}-Q_{,3}\overline{w\theta}-2(K+D)\overline{\theta_{,j}q_{,j}} \tag{24}$$

which indicates that production is balanced by molecular destruction.

Under more unstable conditions ϕ_h probably decreases faster than indicated by Eq. (21), while Fig. 3 suggests that transport remains a source term. Thus for $-z/L>2$ all three terms—transport, production and molecular destruction—are probably significant.

5. The mixed layer

a. Parameterization of terms

Although strictly speaking the AMTEX boundary layer is horizontally inhomogeneous, the mean advective terms in the turbulent second-moment equations are negligible. Furthermore, a Lagrangian time for air passage through the AMTEX area is much larger than a large eddy turnover time in the boundary layer. Thus we can assume the boundary layer turbulence is locally homogeneous and in equilibrium, and use the AMTEX data to examine the $\overline{\theta q}$ budget [Eq. (13)] in the convectively driven mixed layer.

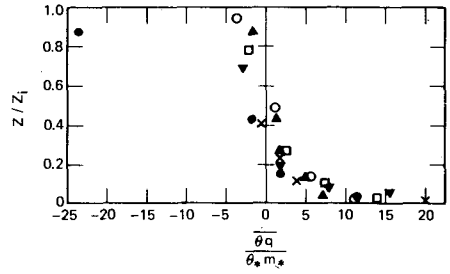

FIG. 4. The $\overline{\theta q}$ profile, made dimensionless with mixed-layer scales, in AMTEX. Symbols as in Fig. 2.

We will nondimensionalize with mixed-layer scales

$$\left.\begin{aligned} w_* &= [(g/T)Q_{0v}z_i]^{\frac{1}{3}} \\ \theta_* w_* &= Q_0 \\ m_* w_* &= M_0 \end{aligned}\right\}. \tag{25}$$

Fig. 4 shows the vertical profile of nondimensional $\overline{\theta q}$ for six AMTEX days. Our scaling collapses the data over most of the mixed layer. The structure in the entrainment region near z_i depends not only on the scaling parameters in Eq. (25) but also on the inversion layer parameters, such as the jumps $\Delta\Theta$ and ΔQ at z_i and the gradients above. We do not have sufficient data near z_i to examine this critically. Furthermore, stratocumulus clouds existed in the upper few hundred meters of the mixed layer over as much as 80% of the area, and temperature and humidity measurements there are affected by cloud water (Lenschow and Pennell, 1974). In addition, flight levels occasionally penetrated through the top of the mixed layer, giving anomalously large values of $\overline{\theta^2}$, $\overline{q^2}$ and $\overline{\theta q}$. The flight leg on 18 February at $z=0.87\ z_i$ is a good example of this (see Figs. 2 and 4). Hence for profiles of terms in the $\overline{\theta q}$ budget we restrict our attention to the region $0.1<z/z_i<0.8$.

Fig. 5 shows the vertical profile of $\overline{w\theta q}$. Note that near the surface it is consistent with the local free convection expression of Eq. (15), which in mixed-layer variables is

$$\overline{w\theta q} = 1.06 m_* w_* \theta_* (z/z_i)^{-\frac{1}{3}}. \tag{26}$$

Eq. (26) follows the data up to $z/z_i \approx 0.2$. For the region $0.1<z/z_i<0.8$ the data scatter about the curve (fit by eye)

$$\overline{w\theta q} = 2.8 m_* w_* \theta_* (1-z/z_i)^2 \tag{27}$$

drawn in Fig. 5. Differentiating Eq. (27) gives an expression for transport in the mixed layer:

$$-(\overline{w\theta q})_{,3} = 5.6(m_* w_* \theta_*/z_i)(1-z/z_i). \tag{28}$$

The production terms in the mixed-layer budget [Eq. (13)] involve both fluxes and mean gradients. The AMTEX flux profiles are shown in Figs. 6 and 7. The temperature flux (Fig. 6) is essentially linear in the region $0<z/z_i<0.8$:

$$\overline{w\theta} \approx Q_0(1-1.5z/z_i). \tag{29}$$

The humidity flux (Fig. 7) falls off much less rapidly with height in the mixed layer. We will parameterize

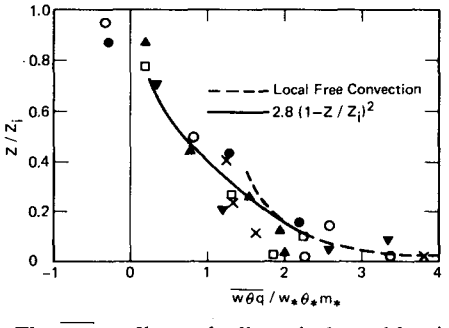

FIG. 5. The $\overline{w\theta q}$ profile, made dimensionless with mixed-layer scales, in AMTEX. The solid curve was used in the parameterized $\overline{\theta q}$ budget. Symbols as in Fig. 2.

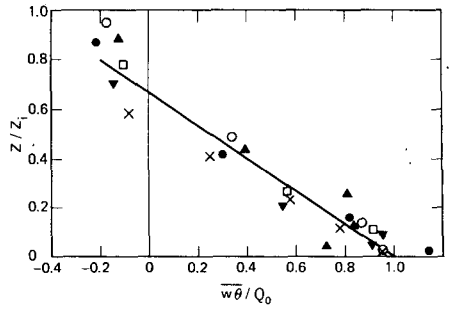

FIG. 6. The sensible heat flux profile, made dimensionless with mixed-layer scales, in AMTEX. The solid line was used in the parameterized $\overline{\theta q}$ budget. Symbols as in Fig. 2.

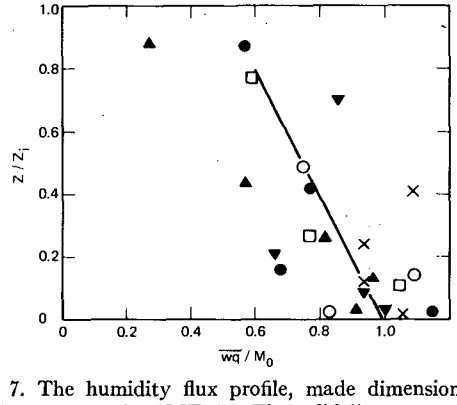

FIG. 7. The humidity flux profile, made dimensionless with mixed-layer scales, in AMTEX. The solid line was used in the parameterized $\overline{\theta q}$ budget. Symbols as in Fig. 2.

the AMTEX profile by

$$\overline{wq}=M_0(1-0.5z/z_i). \tag{30}$$

Our parameterized clear air flux profiles [Eqs. (29) and (30)] are linear interpolations between the surface values and the values induced by entrainment at z_i. The latter are determined by the entrainment velocity w_e and the jumps $\Delta\Theta$ and ΔQ. The value of w_e depends on, among other things, the jump in virtual potential temperature $\Delta\Theta_V$ where Θ_V is defined by

$$\Theta_V=\Theta\left(1+0.61\frac{Q}{\rho}\right). \tag{31}$$

Since Θ_V is always greater above z_i than below ($\Delta\Theta_V$ is positive), entrainment generates negative $\overline{w\theta_V}$ near z_i. This value is typically about -0.2 times the surface value Q_{0V}. Although in principle a clear, inversion-capped mixed layer can have jumps $\Delta\Theta$ and ΔQ of either sign, and hence entrainment-induced values of $\overline{w\theta}$ and $\overline{wq}$ of either sign, in all the AMTEX runs $\Delta\Theta$ was positive and ΔQ negative. Thus the entrainment-induced $\overline{w\theta}$ was negative and $\overline{wq}$ positive. For the AMTEX conditions the profile of $\overline{w\theta_V}$ was determined mainly by $\overline{w\theta}$, so the individual $\overline{wq}$ profiles typically show more variation than $\overline{w\theta}$.

While $(Q/\rho)_{,3}$ in the mixed layer could be fairly accurately estimated, $\Theta_{,3}$ was very small and impossible to determine with any confidence. Instead we used the mixed-layer assumption $\Theta_V=$ constant, which implies to a good approximation for the AMTEX data

$$\Theta_{V,3}=0=\Theta_{,3}+0.61\Theta(Q/\rho)_{,3} \tag{32}$$

$$\Theta_{,3}=-0.61\frac{\Theta}{\rho}\left(Q_{,3}+\frac{Qg}{RT\gamma}\right), \tag{33}$$

where R is the gas constant and $\gamma=1.4$ is the specific heat ratio. For typical values of $Q_{,3}$ this gives a very small, positive $\Theta_{,3}$. On 15 February, for example, $Q_{,3}\approx-1.0\times10^{-3}$ g m^{-4}; from Eq. (33) and the prevailing conditions this gives $\Theta_{,3}\approx0.1$ K km^{-1}. The mixed-layer profiles in Fig. 1 were drawn with these slopes. The Θ and Q profiles for each of the six AMTEX runs analyzed appeared consistent with Eq. (33).

The mean specific humidity gradient in each run was negative. Thus the humidity flux was down the gradient, suggesting the eddy diffusivity parameterization

$$\overline{wq}=-K_q\rho(Q/\rho)_{,3}. \tag{34}$$

We would expect $K_q\approx w_*z_i$ in the mixed layer, and

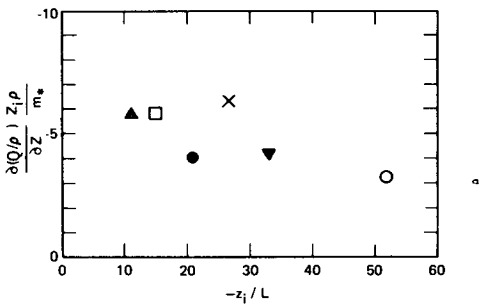

FIG. 8. The mean specific humidity gradient in the AMTEX mixed-layer, made dimensionless with mixed-layer scales, as a function of stability. Symbols as in Fig. 2.

since $\overline{wq}$ scales with M_0 we expect

$$\rho(Q/\rho)_{,3}\approx-\frac{M_0}{w_*z_i}\approx-\frac{m_*}{z_i} \tag{35}$$

in the mixed layer. This is tested in Fig. 8. We will ignore the possible z_i/L dependence suggested by Fig. 8, since the data are limited, and simply average over the runs, finding

$$\rho(Q/\rho)_{,3}=-5\ m_*/z_i. \tag{36}$$

From Eqs. (28), (29), (30), (33) and (36) we can write the $\overline{\theta q}$ budget [Eq. (13)] in the AMTEX mixed layer as

$$(K+D)\overline{\theta_{,j}q_{,j}}=(m_*w_*\theta_*/z_i)[-5A(1-0.5z/z_i)+5(1-1.5z/z_i)+5.6(1-z/z_i)]. \tag{37}$$

Here the parameter $A=(0.61\Theta M_0/\rho Q_0)$ is the ratio of the moisture and sensible temperature contributions to the surface virtual temperature flux. For the AMTEX data A varied between 0.15 and 0.40.

Note that the right side of Eq. (37) changes sign in the mixed layer. The height z_c where this occurs depends only weakly on A, and for the AMTEX conditions one finds from Eq. (37) that $z_c\approx0.8\ z_i$. Thus the molecular destruction term also changes sign at z_c.

Our parameterized AMTEX $\overline{\theta q}$ budget, drawn for $A=0.25$, is shown in Fig. 9. Note that molecular destruction is large over much of the mixed layer.

Whether our parameterizations hold as well for any mixed layer cannot be answered now. It seems necessary to examine in more detail the structure in the entrainment region near z_i and to examine the behavior of the mean profiles in other flows. The recent work by Zeman and Tennekes (1977) should provide a useful framework for analyzing entrainment region structure. Possible starting points for mean profile analysis are the vertical budgets of $\overline{w\theta}$ and $\overline{wq}$. Deardorff (1972) has shown that the $\overline{w\theta}$ budget can ex-

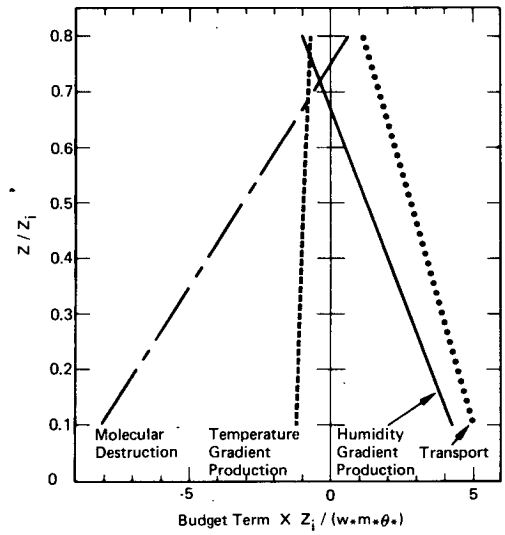

FIG. 9. The parameterized $\overline{\theta q}$ budget in the AMTEX mixed layer for $A=0.25=(0.61\ \Theta\ M_0/\rho Q_0)$.

plain the slightly positive $\Theta_{,3}$ values observed in very unstable, dry mixed layers and possibly the $\overline{wq}$ budget would give similar insight into the behavior of $(Q/\rho)_{,3}$ in the moist case.

b. Relationship to boundary layer growth

We will now show that our parameterized flux profiles [Eqs. (29) and (30)] when combined with jump relations at z_i give reasonable values for the entrainment velocity and the jump in radiative flux at z_i. Following Lilly (1968), Lenschow (1973) and Deardorff (1976) we assume that a linearized version of the equivalent temperature flux

$$\overline{w\theta_e}\equiv\overline{w\theta}+\frac{L}{\rho C_p}\overline{wq} \tag{38}$$

and the total water (water vapor plus liquid and solid water) flux varies linearly with height throughout the mixed layer in both clear and cloudy air except near the top. In the upper hundred meters or so of cloud layers, longwave radiative flux divergence may cause a more rapid decrease in the equivalent temperature flux. Substituting Eqs. (29) and (30) into (38), and using the observed values of Q_0 and M_0, yields

$$\overline{w\theta_e}=Q_{0e}(1-0.73z/z_i). \tag{39}$$

Entrainment of air into the mixed layer results in a nearly discontinuous jump in the fluxes across the turbulent inversion layer capping the mixed layer. According to Lilly (1968), the jump relations for total water (water vapor plus liquid and solid water) and for temperature across the top of the mixed layer are

$$w_e\Delta(Q+L_W)=\overline{-w(q+l_w)_{z_i}} \tag{40}$$

$$w_{ec}\Delta\Theta_V=\overline{-(w\theta_V)_{z_i}} \quad \text{(clear air)}, \tag{41}$$

$$w_{es}\Delta\Theta_e=\overline{-(w\theta_e)_{z_i}}-\frac{\Theta}{T}\Delta R \quad \text{(cloudy air)}, \tag{42}$$

where w_e, w_{ec} and w_{es} are the total, clear air and cloudy air entrainment velocities, respectively (positive for entrainment of air from aloft into the mixed layer), l_w is the water substance fluctuation, $\Delta(Q+L_W)$ is the jump in total water across the mixed-layer top and ΔR is the jump in radiative flux.

Using the observed average values of $M_0=0.17$ g m^{-2} s^{-1} and $\Delta(Q+L_W)=-2.4$ g m^{-3}, and evaluating Eq. (40) with the aid of Eq. (30), we have $w_e=0.035$ m s^{-1}. Substituting Eqs. (29) and (30) into the virtual potential temperature flux equation and using the observed values of Q_0 and M_0 gives

$$\overline{w\theta_V}=Q_{0V}(1-1.3z/z_i). \tag{43}$$

The observed values of Q_{0V} and $\Delta\Theta_V$ are 0.13 m s^{-1} K and 2.7 K, respectively; therefore, $w_{ec}=0.014$ m s^{-1}. The radiative flux term ΔR in Eq. (42) is the most difficult term to estimate. Therefore, we solve Eq. (42) for ΔR. On the basis of flight observations we estimate the cloud cover at 50%. From the estimates of w_e and w_{ec}, we obtain $w_{es}=0.056$ m s^{-1}. Using the observed values of $Q_{0e}=0.45$ m s^{-1} K and $\Delta\Theta_e=-3.3$ K, we have $\Delta R=0.06$ m s^{-1} K. This value agrees well with values calculated with Sasamori's (1968) radiation model using the observed temperature and humidity profiles.

Lilly (1968) suggested that a solid layer of stratocumulus cannot persist for $\Delta\Theta_e\lesssim 0$, while Deardorff (1976) allowed for negative values of $\Delta\Theta_e$ (but not as large as those observed in AMTEX) due to water substance loading. These results are consistent with the observations of scattered to broken decks of stratocumulus.

Inhomogeneity of cloud cover may also be reflected in inhomogeneous boundary layer structure. In the foregoing discussion we have assumed that the measured fluxes, profiles and boundary layer heights are representative of both cloudy and clear areas. LeMone and Pennell (1976) suggest that wide variations in humidity flux profiles related to variations in cloud cover exist in the trade wind boundary layer.

6. Molecular destruction and the θ-q cospectrum

Our data indicate clearly that the $\overline{\theta q}$ budget is balanced by molecular destruction. Under local isot-

ropy we can write the molecular destruction term as

$$2(K+D)\overline{\theta_{,j}q_{,j}}=6(K+D)\overline{\theta_{,1}q_{,1}}$$

$$=(6K+D)\int_0^\infty \kappa_1^2\,\mathrm{Co}_{Tq}(\kappa_1)d\kappa_1. \quad (44)$$

It follows from scaling arguments (Tennekes and Lumley, 1972) that the integral in Eq. (44) must receive its dominant contributions from wavenumbers of the order of η^{-1}. Thus at smaller κ_1, Co_{T_q} cannot fall faster than κ_1^{-2}.

Evidently then the maintenance of $\overline{\theta q}$ occurs in a fashion somewhat analogous to that for $\overline{\theta^2}$ or $\overline{q^2}$. The general features of scalar spectral dynamics are understood: production occurs at large scales, inertial transfer carries the scalar variance to smaller scales, and molecular destruction occurs at the smallest scales. Corrsin (1951) argued that the temperature spectrum Φ_T in the inertial range behaves as

$$\Phi_T=\Phi_T(\epsilon,\kappa,\epsilon_\theta), \quad (45)$$

where ϵ is the dissipation rate of turbulent kinetic energy per unit mass and ϵ_θ the corresponding quantity for $\overline{\theta^2}$. This leads to the well-tested expression for the one-dimensional spectrum

$$\Phi_T=\beta_1\epsilon^{-\frac{1}{3}}\epsilon_\theta\kappa_1^{-5/3}, \quad (46)$$

where $\beta_1\approx 0.4$ (Champagne *et al.*, 1977).

We extend Corrsin's argument to the inertial range of the θ-q spectrum:

$$\mathrm{Co}_{Tq}=\mathrm{Co}_{Tq}(\epsilon,\kappa,\epsilon_{\theta q}), \quad (47)$$

where the destruction rate $\epsilon_{\theta q}$ is

$$\epsilon_{\theta q}=2(K+D)\overline{\theta_{,j}q_{,j}}. \quad (48)$$

Thus we predict for the one-dimensional cospectrum

$$\mathrm{Co}_{Tq}=\gamma_1\epsilon^{-\frac{1}{3}}\epsilon_{\theta q}\kappa_1^{-5/3}, \quad (49)$$

where γ_1 is a constant. However, the arguments given by Zeman and Lumley (1976) suggest γ_1 could vary with the molecular diffusivities K and D, if they differ.

We calculated 40 θ-q cospectra from the AMTEX data, each from runs about 18 km long. They are corrected for the inertial-range phase shift mentioned in Section 2 by multiplying by $[|R(f)|\cos\phi]^{-1}$, where $R(f)$ is the (complex) frequency response function obtained from the Fourier transform of Eq. (8) and ϕ is the phase angle of $R(f)$, using values of $\tau_1=0.03$ s and $\tau_2=1.15$ s. This correction assumes the inertial range is locally isotropic and hence that the θ-q quadrature spectrum vanishes there. Fig. 10 is an example of the θ-q cospectum before and after applying this correction. The corrected cospectrum has an extensive inertial range in agreement with Eq. (49) if $\kappa_1=2\pi f/U$ by Taylor's hypothesis.

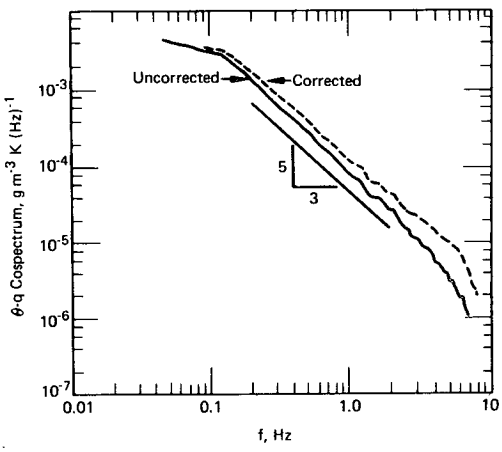

FIG. 10. Frequency cospectrum of humidity (measured with a Lyman-alpha hygrometer and adjusted for the observed time delay) and potential temperature measured on the Electra aircraft. Dashed line has been corrected for both phase shift and attenuation introduced by the thermometer. Both variables are filtered with a 4-pole Butterworth analog filter with a 10 Hz cutoff. The data were obtained from 1344:26 to 1421:45 LT 19 February 1975, at 150 m height over the East China Sea.

Friehe *et al.* (1975) also show a θ-q cospectrum with a $\kappa_1^{-5/3}$ inertial range. Friehe (private communication) has also calculated the θ-q cospectrum for the Minnesota 1973 data reported by Champagne *et al.* (1977). It too has a $\kappa_1^{-5/3}$ inertial range; in addition, we were able to estimate that $\gamma_1\approx 0.5$–0.6 by using the surface layer $\overline{\theta q}$ budget [Eq. (24)] to estimate $\epsilon_{\theta q}$.

Our theory indicates that the $\kappa_1^{-5/3}$ range in the θ-q cospectrum should be as extensive as that for the temperature (or humidity) spectrum. Data do not show this, probably because of instrumental attenuation; it is very difficult to make fast-response, closely spaced θ and q measurements.

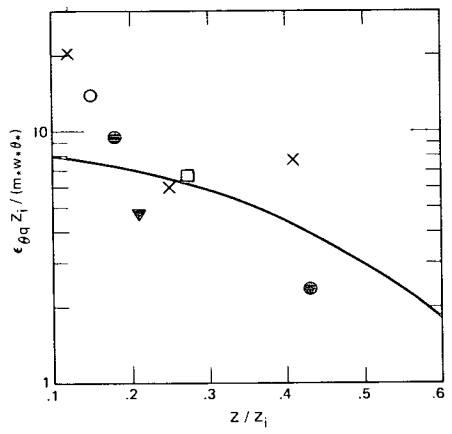

FIG. 11. Molecular destruction rates, made dimensionless with mixed layer scales, from AMTEX. The solid curve is from the parameterized budget (Fig. 9). Symbols as in Fig. 2.

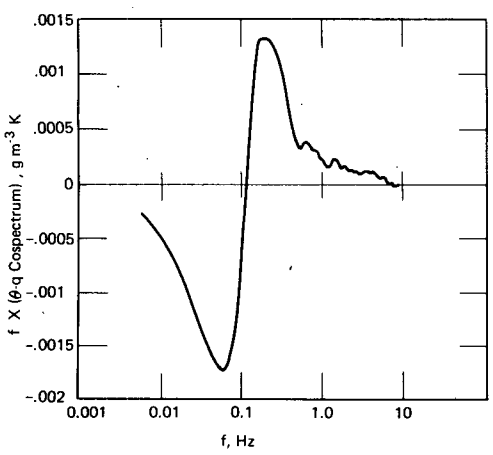

FIG. 12. Cospectrum of θ and q for 24 February 1975 at $z/z_i=0.5$. Cospectral densities are weighted by frequency so that the area between the curve and the x axis is proportional to the covariance.

It was not possible to calculate inertial range θ-q cospectra from all the AMTEX data because of noise problems. However, those available were used for estimates of $\epsilon_{\theta q}$, using Eq. (49) and ϵ values from the inertial range velocity spectra. We used the consensus β_1 value (0.4) for γ_1. The results are shown in Fig. 11, along with the $\epsilon_{\theta q}$ curve from our $\overline{\theta q}$ budget parameterization of Fig. 9. The measured $\epsilon_{\theta q}$ values seem high (compared with the curve) at small z/z_i, perhaps because our parameterization [Eq. (33)] of the mean potential temperature gradient is not accurate there. At z/z_i near 0.1, $\Theta_{,3}$ could still be slightly negative (as in the surface layer), rather than positive (as in the mixed layer). Thus the temperature gradient production term in the budget could be smaller in magnitude or even of the opposite sign near $z\approx 0.1\ z_i$ than indicated in Fig. 9. If so, the parameterized molecular destruction should have larger magnitude there, and hence would agree better with the data of Fig. 11 at small z/z_i. Overall, however, the measured $\epsilon_{\theta q}$ values are consistent with the parameterized curve, giving support to our inertial range cospectral prediction of Eq. (49) with $\gamma_1\approx 0.4$–0.6.

Large eddies complicate the θ-q cospectra (and hence the relationship between $\overline{\theta q}$ and $\epsilon_{\theta q}$), particularly around z_c, the level at which the right-hand side of the parameterized $\overline{\theta q}$ budget in Eq. (37) changes sign. A θ-q cospectrum for $z/z_i=0.5$ appears in Fig. 12. Note that the low-frequency end of the cospectrum is of opposite sign from the higher frequency inertial subrange. This behavior probably reflects the downward transport of warm dry entrained air by kilometer-scale eddies. It also suggests an explanation for the difference between z_c and the height of the $\overline{\theta q}$ zero crossing in Fig. 4. These heights would, of course, be the same if θ and q were correlated in the same sense at all frequencies.

7. Structure parameters

Structure functions are related to spectra through Fourier transforms (Tatarskii, 1971) so the structure parameters are proportional to inertial-range spectral levels. If we consider one-dimensional spectra of temperature and humidity, scaled so that

$$\left.\begin{aligned}\overline{\theta^2}&=\int_0^\infty \Phi_T(\kappa_1)d\kappa_1,\\ \overline{q^2}&=\int_0^\infty \Phi_q(\kappa_1)d\kappa_1,\end{aligned}\right\} \tag{50}$$

then in the inertial range (Wyngaard *et al.*, 1971b)

$$\left.\begin{aligned}\Phi_T&=0.25C_T^2\kappa_1^{-5/3}\\ \Phi_q&=0.25C_q^2\kappa_1^{-5/3}\end{aligned}\right\}. \tag{51}$$

Thus Eq. (49) implies that the θ-q cospectrum, scaled so that

$$\overline{\theta q}=\int_0^\infty \mathrm{Co}_{Tq}(\kappa_1)d\kappa_1 \tag{52}$$

has an inertial range

$$\mathrm{Co}_{Tq}=0.25\,C_{Tq}\kappa_1^{-5/3}. \tag{53}$$

Thus we can relate C_{Tq} to other properties,

$$C_{Tq}=4\gamma_1\epsilon^{-\frac{1}{3}}\epsilon_{\theta q}, \tag{54}$$

in analogy to the well-known results for C_T^2 and C_q^2:

$$\left.\begin{aligned}C_T^2&=4\beta_1\epsilon^{-\frac{1}{3}}\epsilon_\theta\\ C_q^2&=4\beta_1\epsilon^{-\frac{1}{3}}\epsilon_q\end{aligned}\right\}. \tag{55}$$

Eq. (54) provides the basis for describing the behavior of C_{Tq} in the boundary layer. Previous research has revealed the behavior of ϵ both in the surface layer and in the mixed layer (Lenschow, 1974; Kaimal *et al.*, 1976). Our $\overline{\theta q}$ budget results here give considerable insight into the behavior of $\epsilon_{\theta q}$ in the same regions.

Acknowledgments. We wish to acknowledge the excellent support of the NCAR Research Aviation Facility in operating the aircraft and data recording system. We also wish to thank Yunn Pann of NCAR, who did much of the programming and data processing on which the computations are based. We are also grateful to Jeanette Trebing of CIRES for her flawless typing of the manuscript, and to Carl A. Friehe for supplying the Minnesota data used here.

APPENDIX

List of Symbols

Roman symbols

A a parameter in Eq. (43) [$= (0.61\ \Theta M_0/\rho Q_0)$]
C_p specific heat at constant pressure for air
C_v specific heat at constant volume for air
C_n^2, C_T^2, C_q^2 structure parameters for refractive index, temperature and water vapor density, respectively
C_{Tq} joint temperature-humidity structure parameter
Co_{Tq} one-dimensional cospectrum of temperature and humidity
D molecular diffusivity for q
f frequency (Hz)
g acceleration of gravity (9.8 m s^{-2})
h scale height
k von Kármán constant, taken as 0.35
K molecular diffusivity for θ
l turbulence integral scale
L Monin-Obukhov length [$= (-u_*^3 T/kgQ_{0v})$]
l_w fluctuating water substance density (liquid +solid)
L_W mean water substance density at a given level (liquid and solid)
m_* mixed-layer scaling parameter for moisture flux [see Eq. (25)]
M_0 surface moisture flux [$= (\overline{wq})_0$]
n fluctuating refractive index
q fluctuating absolute humidity (g m^{-3})
q_* surface layer scaling parameter for humidity flux (see Eq. 14)
Q_0 surface temperature flux [$= (\overline{w\theta})_0$]
Q at a given level, mean water vapor density (g m^{-3})
$\mathbf{r}$ separation distance between unprimed and primed quantities in Eq. (2)
$r_{\theta q}$ correlation coefficient between θ and q
T mean temperature
T_* surface layer temperature scaling parameter [see Eq. (14)]
t time
u_* friction velocity [see Eq. (14)]
u_j fluctuating velocity component in the j direction
U_j mean velocity component in j direction
w fluctuating vertical velocity
w_* mixed-layer velocity scaling parameter [see Eq. (25)]
w_e entrainment velocity
$\mathbf{x}$ position vector in Eq. (2) for unprimed quantities
$\mathbf{x}+\mathbf{r}$ position vector in Eq. (2) for primed quantities
z height
z_i inversion height

Greek symbols

β_1 one-dimensional scalar spectral constant [Eq. (46)]
γ for air, ratio of C_p/C_v
γ_1 temperature-humidity cospectral constant [Eq. (49)]
Δ jump in a property across z_i
ϵ dissipation rate for turbulence kinetic energy
$\epsilon_q, \epsilon_\theta, \epsilon_{\theta q}$ dissipation rates for $\overline{q^2}$, $\overline{\theta^2}$ and $\overline{\theta q}$, respectively
η Kolmogorov microscale
θ fluctuating temperature
θ_* mixed-layer temperature scaling parameter [see Eq. (25)]
Θ mean potential temperature
ρ mean air density
τ_1, τ_2 time constants in Eq. (8)
ϕ_h dimensionless mean temperature gradient
ϕ_q dimensionless mean moisture gradient, assumed equal to ϕ_h
Φ_T, Φ_q one-dimensional power spectra

Subscripts and superscripts

$(\,)_s$ saturated
$(\,)_0$ surface value
$(\,)'$ at position $\mathbf{x}+\mathbf{r}$
$(\,)_e$ equivalent
$(\,)_v$ virtual

REFERENCES

Buck, A. L., 1976: The variable path Lyman-alpha hygrometer and its operating characteristics. *Bull. Amer. Meteor. Soc.*, **57**, 1113–1118.

Businger, J. A., J. C. Wyngaard, Y. Izumi and E. F. Bradley, 1971: Flux-profile relationships in the atmospheric surface layer. *J. Atmos. Sci.*, **28**, 181–189.

Businger, J. A., 1973: Turbulent transfer in the atmospheric surface layer. *Workshop on Micrometeorology*, D. A. Haugen, Ed., Amer. Meteor. Soc., 67–100.

Champagne, F. H., C. A. Friehe, J. C. LaRue and J. C. Wyngaard, 1977: Flux measurements, flux estimation techniques, and fine scale turbulence measurements in the unstable surface layer over land. *J. Atmos. Sci.*, **34**, 515–530.

Corrsin, S., 1951: On the spectrum of isotropic temperature fluctuations in an isotropic turbulence. *J. Appl. Phys.*, **22**, 469–475.

Deardorff, J. W., 1972: Theoretical expression for the counter-gradient vertical heat flux. *J. Geophys. Res.*, **77**, 5900–5904.

——, 1976: On the entrainment rate of a stratocumulus-topped mixed layer. *Quart. J. Roy. Meteor. Soc.*, **102**, 563–582.

Friehe, C. A., J. C. LaRue, F. H. Champagne, C. H. Gibson and G. F. Dreyer, 1975: Effects of temperature and humidity fluctuations on the optical refractive index in the marine boundary layer. *J. Opt. Soc. Amer.*, **65**, 1502–1511.

Gossard, E. E., 1960: Power spectra of temperature, humidity, and refractive index from aircraft and tethered balloon measurements. *IEEE Trans. Antennas Propagation*, AP-3, 186–201.

Kaimal, J. C., J. C. Wyngaard, D. A. Haugen, O. R. Coté, Y. Izumi, S. J. Caughey and C. J. Readings, 1976: Tur-

bulence structure in the convective boundary layer. *J. Atmos. Sci.*, **33**, 2152–2169.

LeMone, M. A. and W. T. Pennell, 1976: The relationship of trade-wind cumulus distribution to subcloud layer fluxes and structure. *Mon. Wea. Rev.*, **104**, 524–539.

Lenschow, D. H., 1972: The measurement of air velocity and temperature using the NCAR Buffalo aircraft measuring system. NCAR-TN/EDD-74, 39 pp.

——, 1973: Two examples of planetary boundary layer modification over the Great Lakes. *J. Atmos. Sci.*, **30**, 568–581.

——, 1974: Model of the height variation of the turbulence kinetic energy budget in the unstable planetary boundary layer. *J. Atmos. Sci.*, **31**, 465–474.

——, and W. T. Pennell, 1974: On the measurement of in-cloud and wet-bulb temperatures from an aircraft. *Mon. Wea. Rev.*, **102**, 447–454.

Lilly, D. K., 1968: Models of cloud-topped mixed layers under a strong inversion. *Quart. J. Roy. Meteor. Soc.*, **94**, 292–309.

Lumley, J. L., and H. A. Panofsky, 1964: *The Structure of Atmospheric Turbulence.* Interscience-Wiley, 239 pp.

McBean, G. A., and M. Miyake, 1972: Turbulent transfer mechanisms in the atmospheric surface layer. *Quart. J. Roy. Meteor. Soc.*, **98**, 383–398.

McCarthy, J., 1973: A method for correcting airborne temperature data for sensor response time. *J. Appl. Meteor.*, **12**, 211–214.

McGavin, R. E., and M. J. Vetter, 1965: *Humidity and Moisture: Measurement and Control in Science and Industry*, Vol. 2. A. Wexler, Ed. Reinhold, 553–560.

Phelps, G. T., and S. Pond, 1971: Spectra of temperature and humidity fluctuations and of the fluxes of moisture and sensible heat in the marine boundary layer. *J. Atmos. Sci.*, **28**, 918–928.

Sasamori, T., 1968: The radiative cooling calculation for application to general circulation experiments. *J. Appl. Meteor.*, **7**, 721–729.

Swinbank, W. C., and A. J. Dyer, 1967: An experimental study in micrometeorology. *Quart. J. Roy. Meteor. Soc.*, **93**, 494–500.

Tatarskii, V. I., 1971: The effects of the turbulent atmosphere on wave propagation. [NTIS TT 68-50464.]

Tennekes, H., and J. L. Lumley, 1972: *A First Course in Turbulence.* The MIT Press, 300 pp.

Wesely, M. L., 1976: Combined effect of temperature and humidity fluctuations on refractive index. *J. Appl. Meteor.*, **15**, 43–49.

Wyngaard, J. C., and O. R. Coté, 1971: The budgets of turbulent kinetic energy and temperature variance in the atmospheric surface layer. *J. Atmos. Sci.*, **28**, 190–201.

——,—— and Y. Izumi, 1971a: Local free convection, similarity, and the budgets of shear stress and heat flux. *J. Atmos. Sci.*, **28**, 1171–1182.

——, Y. Izumi and S. A. Collins, Jr., 1971b: Behavior of the refractive-index-structure-parameter near the ground. *J. Opt. Soc. Amer.*, **61**, 1646–1650.

Zeman, O., and J. L. Lumley, 1976: Turbulence and diffusion modeling in buoyancy driven mixed layers. *Preprints Third Symp. Atmospheric Turbulence, Diffusion and Air Quality*, Raleigh, Amer. Meteor. Soc., 38–45.

——, and H. Tennekes, 1977: Parameterization of the turbulent energy budget at the top of the daytime atmospheric boundary layer. *J. Atmos. Sci.*, **34**, 111–123.